

INCLUSIVE AND DIFFRACTIVE DIJET PHOTOPRODUCTION IN ULTRAPERIPHERAL Pb-Pb COLLISIONS AT THE LHC

V. GUZEY

University of Jyväskylä, Department of Physics, P.O. Box 35, FI-40014 University of Jyväskylä, Finland and Helsinki Institute of Physics, P.O. Box 64, FI-00014 University of Helsinki, Finland



In this contribution, we summarize NLO pQCD predictions for inclusive and diffractive dijet photoproduction in Pb-Pb UPCs at the LHC. We demonstrate that the theory describes well the preliminary ATLAS data on the inclusive cross section, which probes nuclear parton distributions (PDFs) down to $x_A \approx 0.005$ and which can reduce current uncertainties of the small- x nuclear gluon distribution by approximately a factor of 2. Employing predictions of the leading twist approach to nuclear shadowing for nuclear diffractive PDFs, we calculate the cross section of diffractive dijet photoproduction and show that its x_γ dependence is sensitive to the effect of nuclear shadowing and the mechanism of QCD factorization breaking in hard diffraction. We also find that due to large leading twist nuclear shadowing and restricted kinematics, the diffractive contribution to the inclusive cross section of dijet photoproduction does not exceed 5 – 10%, which helps with an ambiguous interpretation of the ATLAS data.

Keywords: Heavy-ion scattering, ultraperipheral collisions, dijet photoproduction, perturbative QCD, nuclear parton distributions, diffraction, nuclear shadowing

1 Introduction

Jets are collimated sprays of hadrons (π , K , ...) produced in high-energy e^+e^- , lepton-hadron, and hadron-hadron collisions. Jets have been instrumental in establishing quantum chromodynamics (QCD) as the correct theory of the strong interactions and, in particular, its concepts of asymptotic freedom and confinement^{1,2,3}. A classic example of it is 3-jet events observed in e^+e^- annihilation, which has proved the existence of gluons. In perturbative QCD (pQCD), measurements of jets are commonly used to test validity of the QCD collinear factorization theorem, determine the strong coupling constant α_s ^{4,5}, and provide complementary information on parton distribution functions (PDFs)^{6,7}.

In particular, since in electron-proton (ep) deep-inelastic scattering (DIS) and hard hadron scattering, jet cross sections are sensitive to quark and gluon distributions of the target at the same order of the perturbation series in powers of α_s , jet data provide additional constraints on the gluon distribution, which complement those from the total DIS cross section. Global QCD fits of proton PDFs take advantage of it by including data on jet production in ep DIS at HERA, proton-antiproton scattering at Tevatron and proton-proton (pp) scattering at the Large Hadron Collider (LHC)^{8,9,10}. Extending this to nuclear targets, essential constraints on the nuclear gluon distribution have been obtained by employing data on dijet production in proton-nucleus scattering at the LHC¹¹. Similarly, HERA data on dijet photoproduction on the proton enables one to determine the gluon distribution in the real photon more reliably compared to the case, when one only uses the data on the $F_2^\gamma(x, Q^2)$ structure function measured in e^+e^- annihilation¹².

In addition, it has been discussed in the literature that measurements of forward dijet production may aid in searching for small- x Balitsky-Fadin-Kuraev-Lipatov (BFKL) and saturation physics at the LHC^{13,14} and the planned Electron-Ion Collider (EIC) in USA¹⁵. Finally, jets present a Standard Model background for many new physics processes.

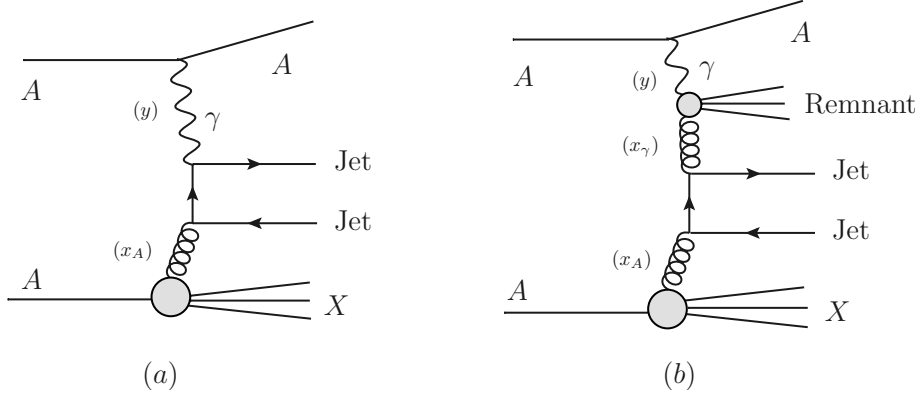


Figure 1 – Typical LO pQCD diagrams for inclusive dijet photoproduction in AA UPCs: (a) direct and (b) resolved photon contributions. The corresponding momentum fractions are given in parenthesis.

Focusing on production of jets by real photons, we notice that while all experimental information on jet photoproduction comes from ep scattering at HERA^{6,7,16}, there is preliminary ATLAS data on dijet photoproduction in Pb-Pb ultraperipheral collisions (UPCs) at the LHC^{17,18}. In UPCs, colliding ions pass each other at large impact parameters and interact via emission of quasi-real photons, which effectively makes the LHC a high-energy and high-intensity photon-nucleus collider¹⁹. So far the emphasis of UPC measurements has been coherent and incoherent production of light and heavy vector mesons. Notably, it has been argued that exclusive photoproduction of charmonium J/ψ mesons in pp UPCs allows one to probe and constrain the gluon density in the proton down to $x_p \approx 3 \times 10^{-6}$ at the resolution scale of the order of the charm quark mass²⁰. In the nucleus case, the data on coherent J/ψ photoproduction in Pb-Pb UPCs have discovered a large nuclear suppression, which can be interpreted in terms of strong gluon nuclear shadowing^{21,22} at $x_A \approx 10^{-3}$ and all the way down to $x_A \approx 10^{-5}$. These findings have nicely confirmed predictions of the leading twist approach (LTA) to nuclear shadowing²³.

Measurements of inclusive and diffractive dijet photoproduction in Pb-Pb UPCs at the LHC allow one to expand the scope of the UPC physics program. Compared to J/ψ production, the theoretical description of the dijet cross section in perturbative QCD is cleaner since it does not involve the charmonium wave function and complications associated with the kinematics of exclusive reactions and generalized parton distributions. In the case of inclusive dijet production, $A + A \rightarrow A + 2\text{jets} + X$, where X denotes the hadronic final state resulting from nucleus dissociation, the dijet cross section probes nuclear and real photon PDFs at large energy scales, which are determined by the jet transverse momentum and, thus, explores the kinematic region complementary to the one in vector meson photoproduction. Requiring that the target nucleus is intact, one can study diffractive dijet photoproduction, $A + A \rightarrow A + 2\text{jets} + X' + A$, which gives an access to novel nuclear diffractive PDFs and which may also shed new light on the mechanism of QCD factorization breaking in hard diffraction.

Pioneering leading-order (LO) pQCD calculations of photoproduction of heavy flavor (bottom) jets²⁴ and heavy quarks²⁵ (see also^{26,27}) in UPCs have demonstrated feasibility and large rates of such measurements in the LHC kinematics.

The rest of this contribution is organized as follows. Section 2 summarizes NLO pQCD predictions for the cross section of inclusive dijet photoproduction in Pb-Pb UPCs at 5.02 TeV, their comparison to the ATLAS data and the magnitude of nuclear modifications as well as the potential of this process to provide additional constraints on nuclear PDFs at small x . In Sec. 3, we present NLO pQCD predictions for diffractive dijet photoproduction in Pb-Pb UPCs at the LHC and discuss sensitivity of the x_γ dependence to the mechanism of the QCD factorization breaking in hard diffraction. We also quantify the diffractive contribution to the cross section of inclusive dijet photoproduction in UPCs. We draw conclusions in Sec. 4.

2 Inclusive dijet photoproduction in Pb-Pb UPCs at the LHC

In the framework of collinear factorization of pQCD, the formalism for calculation of the cross section of inclusive dijet photoproduction is well-established, and results of calculations performed at next-to-leading order (NLO) accuracy successfully describe the available HERA data^{28,29,30,31}. Applying it to UPCs, one can write the cross section of inclusive dijet photoproduction in Pb-Pb UPCs, $A + A \rightarrow A + 2\text{jets} + X$,

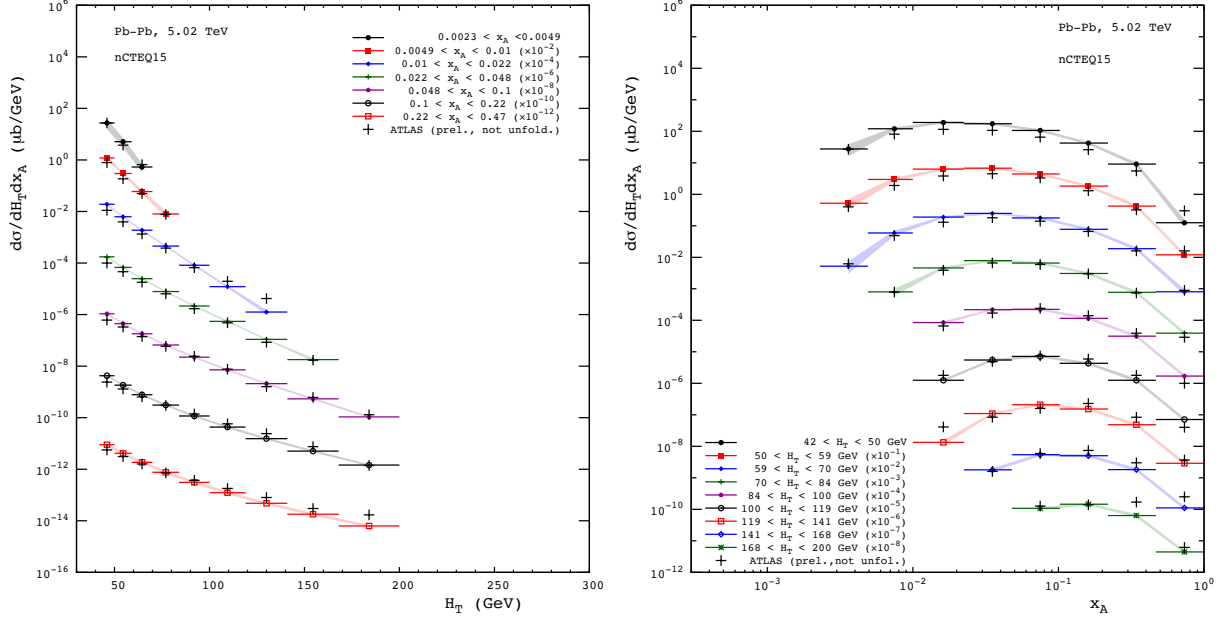


Figure 2 – The cross section of inclusive dijet photoproduction in Pb-Pb UPCs at $\sqrt{s_{NN}} = 5.02$ TeV as a function of $H_T = p_{T,1} + p_{T,2}$ in different bins of x_A (left) and as a function of x_A in bins of H_T (right). The NLO pQCD predictions with the nCTEQ15 nuclear PDFs are compared with the ATLAS preliminary data, see text for details.

as the following convolution ³²,

$$d\sigma(AA \rightarrow A + 2\text{jets} + X) = \sum_{a,b} \int dy \int dx_\gamma \int dx_A f_{\gamma/A}(y) f_{a/\gamma}(x_\gamma, \mu) f_{b/A}(x_A, \mu) d\hat{\sigma}_{ab \rightarrow \text{jets}}, \quad (1)$$

where $f_{\gamma/A}(y)$ is the flux of equivalent photons, $f_{a/\gamma}(x_\gamma, \mu)$ are photon PDFs, $f_{b/A}(x_A, \mu)$ are nuclear PDFs, and $d\hat{\sigma}_{ab \rightarrow \text{jets}}$ is the elementary cross section to produce jets in hard scattering of partons a and b . The longitudinal momentum fractions are y for the photon, x_γ for parton a in the photon, and x_A for parton b in a target nucleus. The PDFs are evaluated at the resolution scale μ , which is usually identified with the jet transverse momentum p_T .

Figure 1 illustrates Eq. (1) by showing typical LO pQCD diagrams for the direct contribution (graph a), where the photon as a whole takes part in the hard reaction, and the resolved contribution (graph b), where a parton of a hadronic fluctuation of the photon (photon PDFs) participates in the hard scattering reaction. The corresponding momentum fractions are given in parenthesis. Separation of the direct and resolved contributions is unambiguous only at LO, where $f_{a/\gamma}(x_\gamma, \mu) = \delta(1 - x_\gamma)$ for the direct term. At NLO, due to renormalization of standard collinear divergences of pQCD, the definition of the direct and resolved terms begins to depend on a choice of the factorization scheme and scale. Nevertheless, the notion of the direct and resolved contributions remains useful.

The photon flux $N_{\gamma/A}(y)$ is usually calculated using the Weizsäcker-Williams equivalent photon approximation combined with the probability for the nuclei not to interact strongly at small impact parameters. However, for purposes of the present analysis, the exact expression can be approximated by the photon flux produced by a relativistic point-like charge Z passing a target at the minimum impact parameter b_{\min} ,

$$N_{\gamma/A}(y) = \frac{2\alpha_{\text{e.m.}} Z^2}{\pi} \frac{1}{y} \left[\zeta K_0(\zeta) K_1(\zeta) - \frac{\zeta^2}{2} (K_0^2(\zeta) - K_1^2(\zeta)) \right], \quad (2)$$

where $\alpha_{\text{e.m.}}$ is the fine-structure constant, $K_{0,1}$ are modified Bessel functions of the second kind, and $\zeta = ym_p b_{\min}$ with m_p the proton mass and $b_{\min} = 14.2$ fm for Pb-Pb UPCs ³³.

The momentum fractions x_γ and x_A in Eq. (1) can be estimated using the measured jet rapidities and transverse momenta. In particular, one can use the following relations

$$x_\gamma = \frac{m_{\text{jets}}}{\sqrt{s_{NN}}} e^{y_{\text{jets}}}, \quad x_A = \frac{m_{\text{jets}}}{\sqrt{s_{NN}}} e^{-y_{\text{jets}}}, \quad (3)$$

where m_{jets} is the invariant mass of the jet system and y_{jets} its rapidity ¹⁷.

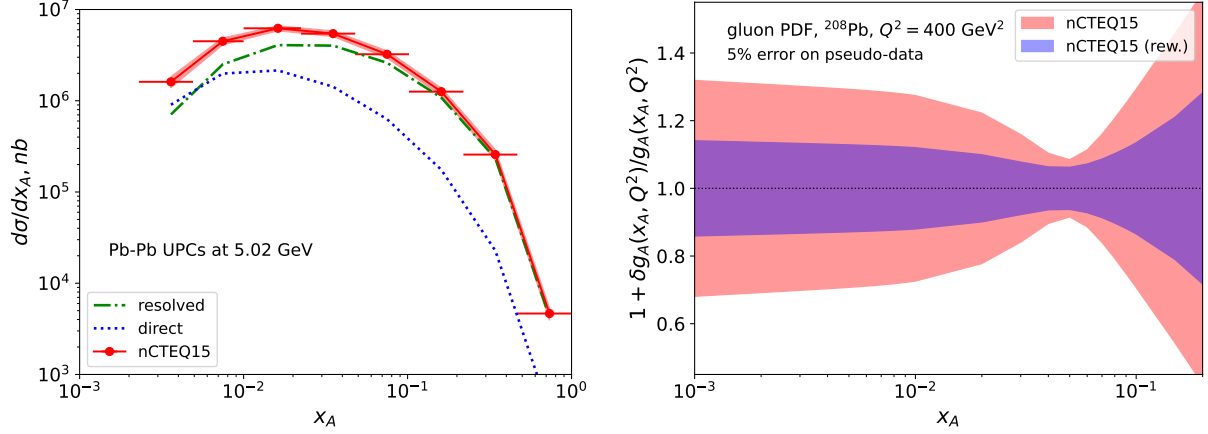


Figure 3 – (Left) NLO pQCD predictions for the cross section of dijet photoproduction in Pb-Pb UPCs at 5.02 TeV as a function of x_A using the nCTEQ15 nuclear PDFs and ATLAS experimental cuts. The curves show separately the direct (dashed) and resolved (dot-dashed) photon contributions as well as their sum (solid). (Right) Relative uncertainties of the nCTEQ15 gluon distribution in ^{208}Pb as a function of x_A at $Q^2 = 400 \text{ GeV}^2$ before (outer pink shaded band) and after (inner blue band) the reweighting using pseudo-data on dijet photoproduction in Pb-Pb UPCs at 5.02 TeV.

Note that Eq. (1) gives the cross section at the level of massless partons and for a comparison with data needs to be supplemented with hadronization corrections. They are usually estimated using Monte Carlo generators, which involve LO matrix elements and include the effects of parton showers^{34,35}.

Figure 2 presents a comparison of the NLO pQCD predictions³² for the cross section of inclusive dijet photoproduction in Pb-Pb UPCs at $\sqrt{s_{NN}} = 5.02 \text{ TeV}$ with the preliminary ATLAS data¹⁷. The calculation used the nCTEQ15 nuclear PDFs³⁶, whose uncertainty propagation is shown by the shaded bands, GRVHO photon PDFs³⁷, and the ATLAS experimental cuts, importantly, $p_{T,1} > 20 \text{ GeV}$ for the leading jet and $p_{T,2} > 15 \text{ GeV}$ for other jets. The left panel shows the distribution in $H_T = p_{T,1} + p_{T,2}$ in different bins of x_A ; the right panel shows the distribution in x_A in bins of H_T . One can see from the figure that the NLO pQCD results correctly reproduce the shape and normalization of the data, which have not been corrected for detector response. Note that in the considered kinematics, the coverage in x_A extends down to $x_A \approx 5 \times 10^{-3}$ at $\mu^2 = (H_T/2)^2$, which provides a certain sensitivity to nuclear PDFs at small x and large μ , see the discussion below.

It is instructive to examine an interplay of the direct and resolved photon contributions to the dijet cross section. The left panel of Fig. 3 shows separately the direct and resolved terms as well as their sum as a function of x_A . One can see from the figure that the resolved contribution dominates for $x_A > 0.01$, while the two contributions are compatible in size for $x_A < 0.01$. This trend is generally expected because the direct photon contribution increases in the $x_\gamma \rightarrow 1$ limit (the values of x_γ and x_A are anti-correlated, see Eq. (3)) and agrees with the expectations based on PYTHIA 8 Monte Carlo framework^{34,35}.

The cross section of dijet photoproduction in Pb-Pb UPCs in Fig. 3 is sensitive to nuclear modifications of nuclear PDFs: its $\approx 10\%$ suppression for $x_A < 0.01$ compared to the impulse approximation estimate is caused by nuclear shadowing and $\approx 20\%$ enhancement around $x_A < 0.1$ by antishadowing of the gluon distribution; it is followed by a 5 – 10% suppression for $x_A > 0.05$ due to the EMC effect, which is built in most of nuclear PDFs.

One can turn this around and quantitatively investigate the potential of this process to further constrain nuclear PDFs using the technique of Bayesian reweighting³⁸. In short, using $N_{\text{rep}} = 10,000$ random replicas of nCTEQ15 error PDFs, $f_{i/A}^k(x, Q^2)$ with i the parton flavor, one can calculate the dijet cross section for each replica $k = 1, 2, \dots, N_{\text{rep}}$ and then determine the statistical weights ω_k for replicas to reproduce observables. The latter was taken to be the dijet cross section calculated using the central nCTEQ15 PDFs, which was assigned a 5 – 15% uncertainty playing the role of experimental errors. After this procedure, the new reweighted central values $\langle f_{i/A}(x, Q^2) \rangle_{\text{new}}$ and uncertainties $\delta \langle f_{i/A}(x, Q^2) \rangle_{\text{new}}$ of

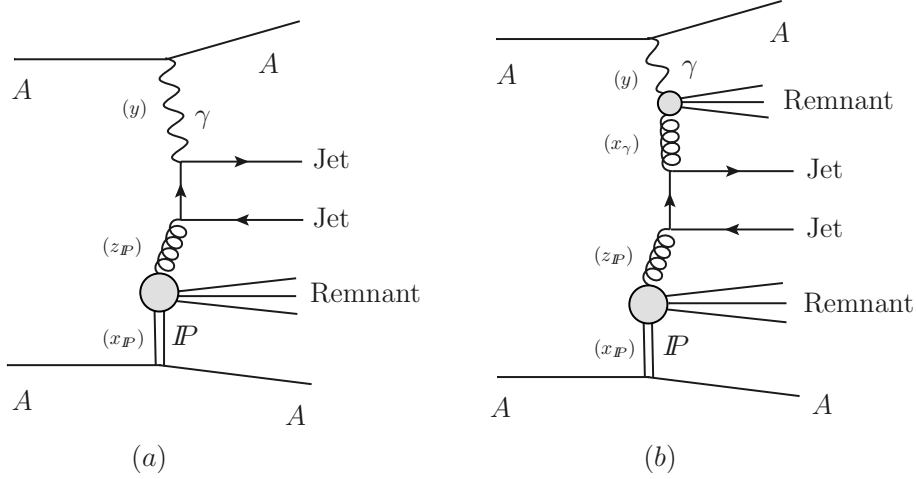


Figure 4 – Typical LO pQCD diagrams for diffractive dijet photoproduction in AA UPCs: (a) direct and (b) resolved photon contributions. The diffractive exchange is denoted by the Pomeron contribution. The corresponding momentum fractions are given in parenthesis.

nuclear PDFs become

$$\begin{aligned} \langle f_{i/A}(x, Q^2) \rangle_{\text{new}} &= \frac{1}{N_{\text{rep}}} \sum_{k=1}^{N_{\text{rep}}} \omega_k f_{i/A}^k(x, Q^2), \\ \delta \langle f_{i/A}(x, Q^2) \rangle_{\text{new}} &= \sqrt{\frac{1}{N_{\text{rep}}} \sum_{k=1}^{N_{\text{rep}}} \omega_k \left(f_{i/A}^k(x, Q^2) - \langle f_{i/A}(x, Q^2) \rangle_{\text{new}} \right)^2}. \end{aligned} \quad (4)$$

The right panel of Fig. 3 illustrates the result of the Bayesian reweighting of the nCTEQ15 gluon distribution in ^{208}Pb at $Q^2 = 400 \text{ GeV}^2$ using the procedure outlined above. It presents the relative uncertainty of the gluon nPDF, $1 + \delta g_A(x_A, Q^2)/g_A(x_A, Q^2)$, as a function of x_A before (outer pink shaded band) and after (inner blue band) the reweighting. One can see from the figure that assigning a 5% uncertainty to the pseudo-data leads to a reduction of uncertainties in the gluon distribution for $x_A < 0.005$ by approximately a factor of 2.

3 Diffractive dijet photoproduction in Pb-Pb UPCs at the LHC

The considerations of the previous section can be extended to diffractive jet photoproduction in heavy-ion UPCs, where one imposes the additional condition that the target nucleus remains intact and recoils elastically. Figure 4 shows typical LO pQCD diagrams for the direct (graph *a*) and resolved (graph *b*) photon contributions, where the vertical double lines denote the diffractive exchange (Pomeron flux) labeled “ P ”.

Unlike the inclusive case, UPC cross sections corresponding to coherent underlying photon-nucleus scattering receive contributions from both left-moving and right-moving colliding ions, which introduces a well-known two-fold ambiguity between the photon energy and rapidity of the final dijet system. Generalizing Eq. (1), the contribution of the right-moving photon source to the cross section of diffractive dijet photoproduction in Pb-Pb UPCs, $A + A \rightarrow A + 2\text{jets} + X' + A$, where X' includes hadronic debris of the “Pomeron” and photon, can be written in the following form³⁹

$$\begin{aligned} d\sigma(AA \rightarrow A + 2\text{jets} + X' + A)^{(+)} &= \sum_{a,b} \int dt \int dx_{\mathcal{P}} \int dz_{\mathcal{P}} \int dy \int dx_{\gamma} \\ &\times f_{\gamma/A}(y) f_{a/\gamma}(x_{\gamma}, \mu) f_{b/A}^{D(4)}(x_{\mathcal{P}}, z_{\mathcal{P}}, t, \mu) d\hat{\sigma}_{ab \rightarrow \text{jets}}. \end{aligned} \quad (5)$$

The contribution of the left-moving photon source is obtained from Eq. (5) by inverting signs of the jet rapidities. In Eq. (5), $f_{b/A}^{D(4)}(x_{\mathcal{P}}, z_{\mathcal{P}}, t, \mu)$ denote the nuclear diffractive PDFs, which represent the conditional probability to find parton b with the momentum fraction $z_{\mathcal{P}}$ with respect to the diffractive exchange (Pomeron) carrying the momentum fraction $x_{\mathcal{P}}$, provided that the nucleus remains intact and

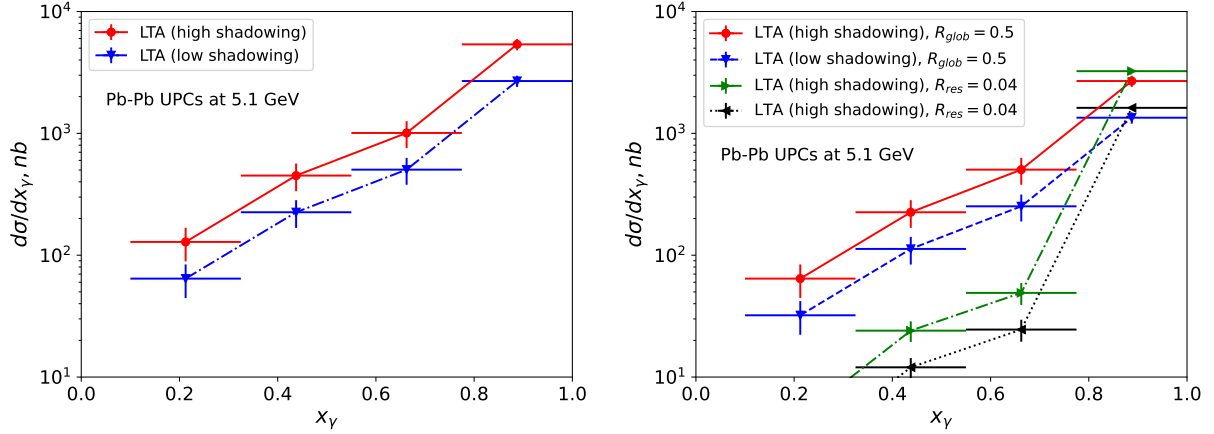


Figure 5 – NLO pQCD predictions for the cross section of diffractive dijet photoproduction in Pb-Pb UPCs at 5.1 TeV as a function of x_γ . The results are obtained using LTA predictions for nuclear diffractive PDFs (“high shadowing” and “low shadowing” versions) and assuming either no QCD factorization breaking in hard diffraction (left) or two scenarios of it realized through the suppression factors R_{glob} and R_{res} (right), see text for details.

recoils elastically with the momentum transfer t . The momentum fractions involved in Eq. (5) are shown in parenthesis in Fig. 4.

Similarly to usual nuclear PDFs, nuclear diffractive PDFs are subject to nuclear modifications, notably, due to nuclear shadowing. The leading twist approach to nuclear shadowing²³ makes definite predictions for $f_{b/A}^{D(4)}$, which are characterized by their strong suppression at small x . It can be quantified by introducing the suppression factor R_b with respect to $f_{b/A}^{D(4)}$ evaluated in the impulse approximation,

$$f_{b/A}^{D(4)}(x_{\mathbb{P}}, z_{\mathbb{P}}, t, \mu) = R_b(x_{\mathbb{P}}, z_{\mathbb{P}}, \mu) A^2 F_A^2(t) f_{b/p}^{D(4)}(x_{\mathbb{P}}, z_{\mathbb{P}}, t = 0, \mu), \quad (6)$$

where $F_A(t)$ is the nucleus form factor and $f_{b/p}^{D(4)}$ is the diffractive PDFs of the proton. An examination of R_b shows that it rather weakly depends on flavor b , the light-cone momentum fractions $x_{\mathbb{P}}$ and $z_{\mathbb{P}}$ (provided that $x_{\mathbb{P}}$ is sufficiently small), and the resolution scale μ . Hence, for the purpose of estimating yields of this process, one can approximate R_b by a single number^{39,40}

$$R_b(x_{\mathbb{P}}, z_{\mathbb{P}}, \mu) \approx 0.08 - 0.16, \quad (7)$$

where the upper and lower values correspond to the “high shadowing” and “low shadowing” scenarios, respectively. This spread in the values for R_b reflects a significant theoretical uncertainty of LTA predictions for nuclear diffractive PDFs, for a detailed discussion, see⁴⁰.

The left panel of Fig. 5 presents NLO pQCD predictions for the cross section of diffractive dijet photoproduction in Pb-Pb UPCs at 5.1 TeV as a function of x_γ using the LTA results for nuclear diffractive PDFs, see Eqs. (6) and (7), $p_{T,1} > 20$ GeV for the leading jet and $p_{T,2} > 18$ GeV for sub-leading jets and other otherwise generic cuts specified in³⁹. The upper and lower curves corresponds to the “high shadowing” and “low shadowing” LTA predictions, respectively. The horizontal lines show the width of bins in x_γ , and the vertical bars quantify the effect of the variation of the hard scale of the process in the $p_{T,1}/2 < \mu < 2p_{T,1}$ interval. One can see from the figure that the uncertainty due to the scale variation is smaller than the uncertainty in the value of R_b . Overall, the figure shows that the predicted yields are significant demonstrating feasibility of such measurements.

Analyses of diffractive dijet photoproduction in ep scattering at HERA have shown that the QCD factorization theorem for hard diffraction⁴¹ is violated and NLO pQCD calculations overestimate the cross sections measured by the ZEUS and H1 collaborations at HERA by a approximately a factor of 2, see details in⁴². The pattern of this factorization breaking is yet unknown since a good description of the data can be achieved by introducing a global suppression factor $R_{\text{glob}} = 0.5$ or the suppression factor $R_{\text{res}} = 0.34$ for the resolved photon contribution only, or the flavor-dependent and x_γ -dependent suppression factor interpolating between R_{glob} and R_{res} , see⁴³.

As a consequence, one of the most sensitive observables to various scenarios of factorization breaking is the distribution in the momentum fraction x_γ . Thus, it has been argued in³⁹ that measurements of

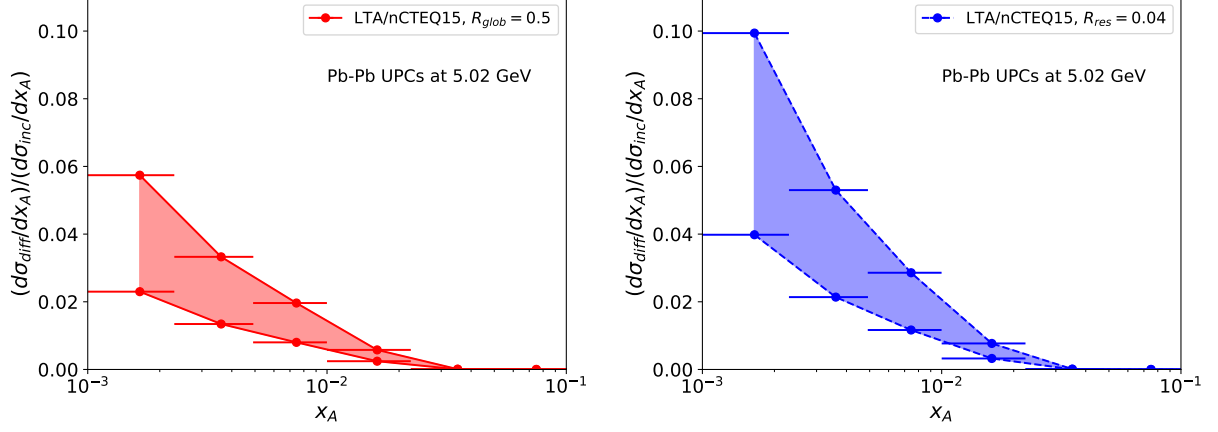


Figure 6 – NLO pQCD predictions for the ratio of the cross sections of diffractive to inclusive dijet photoproduction in Pb-Pb UPCs at 5.02 TeV as a function of x_A . The calculation uses LTA predictions for nuclear diffractive PDFs (the shaded bands represent the theoretical uncertainty), the nCTEQ15 nuclear PDFs, and two scenarios of the QCD factorization breaking in hard diffraction realized through the global suppression factor $R_{\text{glob}} = 0.5$ (left panel) and the direct photon suppression factor $R_{\text{res}} = 0.04$ (right panel).

the x_γ dependence of the cross section of diffractive dijet photoproduction in UPCs at the LHC may help to shed new light on this phenomenon.

The right panel of Fig. 5 illustrates the effect of the QCD factorization breaking for hard diffraction on NLO pQCD predictions for the cross section of diffractive dijet photoproduction in Pb-Pb UPCs at 5.1 TeV as a function of x_γ . These predictions are obtained by rescaling the result of Eq. (5) either by the global suppression factor of $R_{\text{glob}} = 0.5$ or by suppressing only the resolved photon term by the factor of $R_{\text{res}} = 0.04$. The latter value is estimated using the Glauber model for ρ meson-nucleus scattering, see details in ⁴³. One can see from the figure that the two prescriptions for factorization breaking result in rather distinct shapes of the x_γ distribution, which supports its potential to discriminate between these two scenarios.

The ATLAS measurement of inclusive dijet photoproduction in Pb-Pb UPCs was performed in the so-called “0nXn” event topology, which required a particular number of forward neutrons in zero degree calorimeters (ZDCs), namely, no neutrons in one direction and one or more neutrons in the opposite direction. This condition has totally eliminated the contribution of coherent nuclear diffraction, which is part of nuclear PDFs. It raises the practical question of the magnitude of the diffractive contribution to inclusive dijet photoproduction in UPCs.

The analysis ⁴⁴ has shown that the diffractive contribution to inclusive dijet photoproduction in Pb-Pb UPCs in the ATLAS kinematics does not exceed 5 – 10% at small x_A . It is illustrated in Fig. 6 showing the ratio of the cross sections of diffractive to inclusive dijet photoproduction in Pb-Pb UPCs at 5.02 TeV, $(d\sigma_{\text{diff}}/dx_A)/(d\sigma_{\text{inc}}/dx_A)$, as a function of x_A . The calculation uses the LTA predictions for nuclear diffractive PDFs entering the diffractive cross section (the shaded bands quantify the theoretical uncertainty, see Fig. 5) and the nCTEQ15 nuclear PDFs for the inclusive cross section. The effect of the QCD factorization breaking for hard diffraction (see the discussion above) is included through either the global suppression factor $R_{\text{glob}} = 0.5$ (left panel) or the direct photon suppression factor $R_{\text{res}} = 0.04$ (right panel). The two scenarios of the factorization breaking lead to different magnitudes and shapes of the dependence of $(d\sigma_{\text{diff}}/dx_A)/(d\sigma_{\text{inc}}/dx_A)$ on x_A .

The small value of the $(d\sigma_{\text{diff}}/dx_A)/(d\sigma_{\text{inc}}/dx_A)$ ratio is predominantly an effect of the restricted kinematics with large $p_{T,1} > 20$ GeV and not-sufficiently small $x_A > 0.001$ and large relative suppression of nuclear diffractive PDFs by leading twist nuclear shadowing ⁴⁰. Thus, the diffractive contribution and the ensuing ambiguity in the determination of the photon-emitting nucleus (ambiguity in the invariant photon-nucleon energy $W_{\gamma p}$) can be safely neglected in the kinematics of the ATLAS measurement.

To enhance the diffractive signal, one needs to expand the kinematic coverage by primarily lowering p_T of jets. For instance, using $p_{T,1} > 10$ GeV and $p_{T,2} > 5\text{--}7$ GeV, one can reach $(d\sigma_{\text{diff}}/dx_A)/(d\sigma_{\text{inc}}/dx_A) = 10\text{--}20\%$ at $x_A \approx 5 \times 10^{-4}$. In the case of pp UPCs at 13 TeV, where the collision energy is larger and there is no nuclear suppression of diffractive PDFs by nuclear shadowing, the ratio of the diffractive and inclusive cross sections of dijet production is sizable, $(d\sigma_{\text{diff}}/dx_p)/(d\sigma_{\text{inc}}/dx_p) \approx 10\text{--}15\%$ at $x_p \approx 5 \times 10^{-4}$.

4 Summary and outlook

Photoproduction of jets is a standard tool of perturbative QCD, which provides important information on parton distributions of the proton, the real photon, and nuclei. Within the framework of collinear factorization of pQCD, NLO calculations describe well the available data on dijet photoproduction in ep scattering at HERA. Application of this framework to photon-nucleus scattering in heavy-ion UPCs at the LHC can be used to obtain complementary constraints on nuclear PDFs, measure for the first time nuclear diffractive PDFs and shed new light on the mechanism of QCD factorization breaking in hard diffraction.

Using NLO pQCD, we calculate the cross section of inclusive dijet photoproduction in Pb-Pb UPCs at 5.02 TeV at the LHC and demonstrate that it describes well the preliminary ATLAS data. We show that this cross section probes nuclear PDFs down to $x_A \approx 0.005$ and, when used in the form of pseudo-data in a Bayesian analysis, can reduce the current small- x uncertainties of the state-of-art nuclear PDFs by approximately a factor of 2.

Considering coherent nuclear scattering and using predictions of the leading twist approach (LTA) to nuclear shadowing for nuclear diffractive PDFs, we make NLO pQCD predictions for the cross section of diffractive dijet photoproduction in Pb-Pb UPCs at 5.1 TeV. We show that its distribution in the photon momentum fraction x_γ is sensitive to both the effect of nuclear shadowing in nuclear diffractive PDFs and the mechanism of QCD factorization breaking in hard diffraction. In particular, it allows one to discriminate between the two scenarios of factorization breaking, where its effect is introducing either through the global suppression factor $R_{\text{glob}} = 0.5$ or the resolved photon suppression factor $R_{\text{res}} = 0.04$. We also show that due to large leading twist nuclear shadowing and restricted ATLAS kinematics (large jet transverse momentum p_T and not sufficiently small x_A), the diffractive contribution to the inclusive cross section of dijet photoproduction does not exceed 5 – 10%. It means that one can expect only small corrections of the ATLAS (and other similar) data for the excluded diffractive contribution, which simplifies their interpretation in terms of usual nuclear PDFs.

Both inclusive and diffractive dijet photoproduction in Pb-Pb UPCs at the LHC can be viewed as precursors of analogous measurement in photon-nucleus scattering at the planned Electron-Ion Collider (EIC) ^{45,46}.

Acknowledgments

The research of V.G. was funded by the Academy of Finland project 330448, the Center of Excellence in Quark Matter of the Academy of Finland (projects 346325 and 346326), and the European Research Council project ERC-2018-ADG-835105 YoctoLHC. The research of M.S. was supported by the US Department of Energy Office of Science, Office of Nuclear Physics under Award No. DE- FG02-93ER40771.

References

1. G. P. Salam, [arXiv:1011.5131 [hep-ph]].
2. S. Sapeta, Prog. Part. Nucl. Phys. **89**, 1-55 (2016) [arXiv:1511.09336 [hep-ph]].
3. E. Laenen, [arXiv:1708.00770 [hep-ph]].
4. H. Abramowicz *et al.* [ZEUS], Nucl. Phys. B **864**, 1-37 (2012) [arXiv:1205.6153 [hep-ex]].
5. V. Andreev *et al.* [H1], Eur. Phys. J. C **75**, no.2, 65 (2015) [arXiv:1406.4709 [hep-ex]].
6. M. Klein and R. Yoshida, Prog. Part. Nucl. Phys. **61**, 343-393 (2008) [arXiv:0805.3334 [hep-ex]].
7. P. Newman and M. Wing, Rev. Mod. Phys. **86**, no.3, 1037 (2014) [arXiv:1308.3368 [hep-ex]].
8. S. Chekanov *et al.* [ZEUS], Eur. Phys. J. C **42**, 1-16 (2005) [arXiv:hep-ph/0503274 [hep-ph]].
9. R. D. Ball *et al.* [NNPDF], Eur. Phys. J. C **82**, no.5, 428 (2022) [arXiv:2109.02653 [hep-ph]].
10. T. J. Hou, J. Gao, T. J. Hobbs, K. Xie, S. Dulat, M. Guzzi, J. Huston, P. Nadolsky, J. Pumplin and C. Schmidt, *et al.* Phys. Rev. D **103**, no.1, 014013 (2021) [arXiv:1912.10053 [hep-ph]].
11. K. J. Eskola, P. Paakkinen, H. Paukkunen and C. A. Salgado, Eur. Phys. J. C **82**, no.5, 413 (2022) [arXiv:2112.12462 [hep-ph]].
12. W. Slominski, H. Abramowicz and A. Levy, Eur. Phys. J. C **45**, 633-641 (2006) [arXiv:hep-ph/0504003 [hep-ph]].
13. M. Hentschinski, C. Royon, M. A. Peredo, C. Baldenegro, A. Bellora, R. Boussarie, F. G. Celiberto, S. Cerci, G. Chachamis and J. G. Contreras, *et al.* Acta Phys. Polon. B **54**, no.3, 3-A2 (2023) [arXiv:2203.08129 [hep-ph]].

14. E. Iancu, A. H. Mueller, D. N. Triantafyllopoulos and S. Y. Wei, *Eur. Phys. J. C* **83**, no.11, 1078 (2023) [arXiv:2304.12401 [hep-ph]].
15. R. Boussarie, H. Mäntysaari, F. Salazar and B. Schenke, *JHEP* **09**, 178 (2021) [arXiv:2106.11301 [hep-ph]].
16. J. M. Butterworth and M. Wing, *Rept. Prog. Phys.* **68**, 2773-2828 (2005) [arXiv:hep-ex/0509018 [hep-ex]].
17. [ATLAS], “Photo-nuclear dijet production in ultra-peripheral Pb+Pb collisions,” ATLAS-CONF-2017-011.
18. [ATLAS], “Photo-nuclear jet production in ultra-peripheral Pb+Pb collisions at $\sqrt{s_{NN}} = 5.02$ TeV with the ATLAS detector,” ATLAS-CONF-2022-021.
19. A. J. Baltz, G. Baur, D. d’Enterria, L. Frankfurt, F. Gelis, V. Guzey, K. Hencken, Y. Kharlov, M. Klasen and S. R. Klein, *et al. Phys. Rept.* **458**, 1-171 (2008)
20. C. A. Flett, A. D. Martin, M. G. Ryskin and T. Teubner, *Phys. Rev. D* **102**, 114021 (2020) [arXiv:2006.13857 [hep-ph]].
21. V. Guzey, E. Kryshen, M. Strikman and M. Zhalov, *Phys. Lett. B* **726**, 290-295 (2013) [arXiv:1305.1724 [hep-ph]].
22. V. Guzey and M. Zhalov, *JHEP* **10**, 207 (2013) [arXiv:1307.4526 [hep-ph]].
23. L. Frankfurt, V. Guzey and M. Strikman, *Phys. Rept.* **512**, 255-393 (2012) [arXiv:1106.2091 [hep-ph]].
24. M. Strikman, R. Vogt and S. N. White, *Phys. Rev. Lett.* **96**, 082001 (2006) [arXiv:hep-ph/0508296 [hep-ph]].
25. S. R. Klein, J. Nystrand and R. Vogt, *Phys. Rev. C* **66**, 044906 (2002) [arXiv:hep-ph/0206220 [hep-ph]].
26. V. P. Goncalves, M. V. T. Machado and A. R. Meneses, *Phys. Rev. D* **80**, 034021 (2009) [arXiv:0905.2067 [hep-ph]].
27. V. P. Gonçalves, G. Sampaio dos Santos and C. R. Sena, *Nucl. Phys. A* **976**, 33-45 (2018) [arXiv:1711.04497 [hep-ph]].
28. S. Frixione and G. Ridolfi, *Nucl. Phys. B* **507**, 315-333 (1997) [arXiv:hep-ph/9707345 [hep-ph]].
29. M. Klasen and G. Kramer, *Z. Phys. C* **76**, 67-74 (1997) [arXiv:hep-ph/9611450 [hep-ph]].
30. P. Aurenche, L. Bourhis, M. Fontannaz and J. P. Guillet, *Eur. Phys. J. C* **17**, 413-421 (2000) [arXiv:hep-ph/0006011 [hep-ph]].
31. M. Klasen, *Rev. Mod. Phys.* **74**, 1221-1282 (2002) [arXiv:hep-ph/0206169 [hep-ph]].
32. V. Guzey and M. Klasen, *Phys. Rev. C* **99**, no.6, 065202 (2019) [arXiv:1811.10236 [hep-ph]].
33. J. Nystrand, *Nucl. Phys. A* **752**, 470-479 (2005) [arXiv:hep-ph/0412096 [hep-ph]].
34. I. Helenius, *PoS HardProbes2018*, 118 (2018) [arXiv:1811.10931 [hep-ph]].
35. I. Helenius and C. O. Rasmussen, *Eur. Phys. J. C* **79**, no.5, 413 (2019) [arXiv:1901.05261 [hep-ph]].
36. K. Kovarik, A. Kusina, T. Jezo, D. B. Clark, C. Keppel, F. Lyonnet, J. G. Morfin, F. I. Olness, J. F. Owens and I. Schienbein, *et al. Phys. Rev. D* **93**, no.8, 085037 (2016) [arXiv:1509.00792 [hep-ph]].
37. M. Gluck, E. Reya and A. Vogt, *Phys. Rev. D* **46**, 1973-1979 (1992)
38. V. Guzey and M. Klasen, *Eur. Phys. J. C* **79**, no.5, 396 (2019) [arXiv:1902.05126 [hep-ph]].
39. V. Guzey and M. Klasen, *JHEP* **04**, 158 (2016) [arXiv:1603.06055 [hep-ph]].
40. V. Guzey and M. Strikman, [arXiv:2403.08342 [hep-ph]].
41. J. C. Collins, *Phys. Rev. D* **57**, 3051-3056 (1998) [erratum: *Phys. Rev. D* **61**, 019902 (2000)] [arXiv:hep-ph/9709499 [hep-ph]].
42. M. Klasen and G. Kramer, *Eur. Phys. J. C* **70**, 91-106 (2010) [arXiv:1006.4964 [hep-ph]].
43. V. Guzey and M. Klasen, *Eur. Phys. J. C* **76**, no.8, 467 (2016) [arXiv:1606.01350 [hep-ph]].
44. V. Guzey and M. Klasen, *Phys. Rev. D* **104**, no.11, 114013 (2021) [arXiv:2012.13277 [hep-ph]].
45. V. Guzey and M. Klasen, *Phys. Rev. C* **102**, no.6, 065201 (2020) [arXiv:2003.09129 [hep-ph]].
46. V. Guzey and M. Klasen, *JHEP* **05**, 074 (2020) [arXiv:2004.06972 [hep-ph]].